JOURNAL OF MATERIALS SCIENCE 7 (1972) 34–39

Initial Dislocation Distributions in Tungsten Fibre-Copper Composites

K. K. CHAWLA, M. METZGER
Department of Metallurgy and Mining Engineering and Materials Research Laboratory, University of Illinois at Urbana-Champaign, Urbana, Illinois 61801, USA

Etch-pit studies of composites consisting of small volume fractions of tungsten wires into which a copper matrix had been introduced by vacuum infiltration showed the dislocation density in the single crystal matrix to increase with volume fraction of fibre and to rise to high values toward the fibre-matrix interface. The dislocation distributions, which resulted from strains arising due to differential shrinkage, were interpreted in terms of a contribution, independent of fibre fraction, due to transverse strains which fall off with distance from the fibre and a second one due to axial strain which increases with fibre fraction but is invariant with distance from the fibre. Part of the axial adjustment is accomplished by interface shear.

1. Introduction

A central question in regard to the mechanical properties of metal-matrix fibre-reinforced composites is the behaviour of the matrix. This may differ from that of the unreinforced matrix because of either rheological fibre-matrix interaction during straining or of fibre influence on matrix structure during preparation of the composite. The second question can be investigated by direct observations of grain and dislocation structure, but because of the difficulty of preparing specimens for the latter in most systems, only a few such observations had been made [1, 2] until recently [3, 4], and only one relatively systematic study (on aluminium-stainless steel) has been reported [3]. In general, stresses due to differential shrinkage on cooling from the fabricating temperature are expected to produce some degree of plastic strain and enhanced dislocation density in the matrix unless this anneals fully near room temperature. The present work made use of the copper-tungsten system with a single crystal matrix to investigate matrix structure by dislocation etch pitting, low fibre fractions and large fibres being employed to ensure the availability of large matrix areas for observation even if a region near the fibre were not accessible for study.

2. Experimental Procedure

Specimens were prepared in a vacuum furnace at $\sim 10^{-5}$ torr by infiltrating molten American Smelting and Refining 99.999+ % copper into a bundle of cleaned tungsten wires held by copper foil spacers in a spectroscopically pure graphite mould and then solidifying at 2 cm h^{-1}, the furnace being similar to one described for growing copper crystals [5]. The specimen, 3 mm diameter × 36 mm long, remained near the melting point 5 to 6 h after solidifying and then cooled to room temperature in about 6 h. The General Electric 218 CS tungsten wire was chosen with a large (228 μm) diameter to maximise the size of the free matrix region for a given fibre fraction (V_f). The matrix region associated with each fibre then extended radially 176 μm at $V_f = 15\%$ and 1470 μm for a one-wire specimen, $V_f = 0.5\%$.

The specimens were sectioned by EDM on the primary (1 1 1) plane of the copper single-crystal matrix using a $\frac{1}{4}$ mm copper wire and a slow cutting speed. The spark-erosion damage was restricted to a layer 200 μm or less thick. In polishing, problems were encountered in retaining a flat (1 1 1) surface for etching because the tungsten wires were attacked only slightly by the chemical polishing solution and were left protruding from the section, and they tended to form a galvanic cell with the copper and produce some preferential attack of the adjacent matrix. Flatness was best preserved by chemically polishing on a cloth until the wires protruded

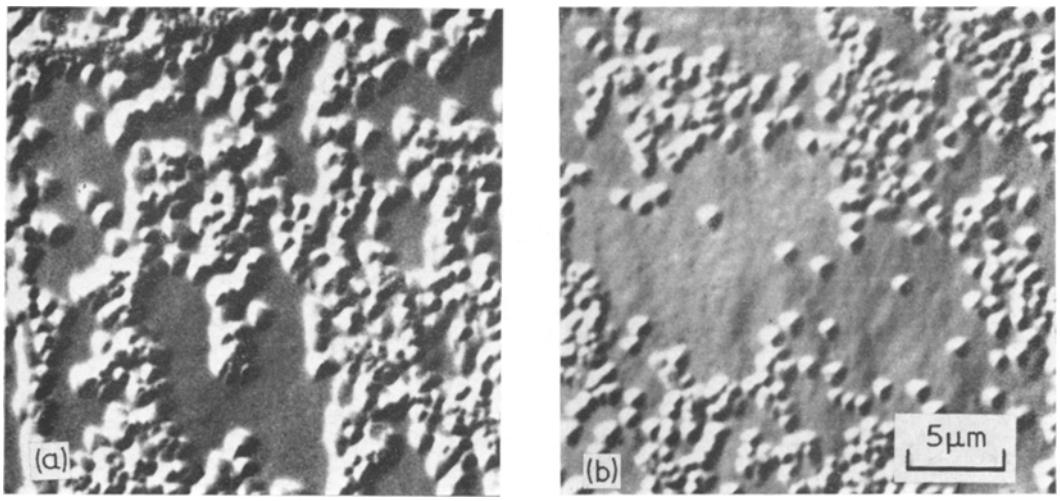

Figure 1 Etch pits on the matrix primary plane in an as-grown $V_f = 15\%$ composite at (a) 70 μm, (b) 190 μm from the interface.

too far for this. A cotton sheet was stretched over a grooved Teflon base containing the polishing solution [6] (equal parts by volume of 70% nitric acid, glacial acetic acid and 86% orthophosphoric acid), and the specimens, mounted in small copper holders with a low-melting (45°C) wax, were moved gently over the cloth until a layer of about 200 μm was removed. Up to another 200 μm was removed by simple immersion in the polishing solution, sometimes with a final electropolishing treatment in an orthophosphoric acid bath. In general, the surface was close enough to (1 1 1) for etching up to 20 to 30 μm from the fibre. The polished specimens were rinsed with 10% H_3PO_4, 5% KCN and water [7] and dried with methanol. They were then etched lightly with Livingston's dislocation etch for copper [8]. The tungsten wires caused no difficulty in rinsing and etching.

Etch-pit distributions were examined by scanning electron microscopy, in which adequate contrast could be obtained in the backscattered electron image at 25 kV and pits resolved up to fairly high densities in a lightly etched specimen. Relatively low density specimens were also etched more heavily for reassurance that there was no loss of pits.

3. Results

Matrix dislocation densities in primary plane sections were much higher than those of unreinforced copper crystals. Most of these dislocations lay in the walls of a more or less well-defined cell structure having dimensions of the order of 10 μm, as in fig. 1a. However, narrow sub-boundaries in the composites defining subgrains $\lesssim 100$ μm in size did not appear different in character from the sub-boundaries in unreinforced crystals although the subgrain size was smaller. Near the fibres the cell structure was better defined, the cell size somewhat smaller and the dislocation density high, figs. 1a and b; the usual limitation on how close observations could be made was, however, not pit resolution but surface deviation from (1 1 1). Away from the fibre, the extent to which cell structure was developed increased with fibre fraction and was apparently not strongly sensitive to crystal orientation. Two specimens sectioned also on the cross-glide plane showed similar structures and pit densities little if any higher. All further studies were made on primary plane sections.

Dislocation density measurements were made along the major and minor axes of the ellipses concentric to the elliptical section of the fibre, fig. 2. Every resolved pit was counted. The backscattered electron images were such that pits less than 0.3 μm apart could not normally be resolved. Thus a local density greater than 10^9 cm^{-2} in a dense cluster would have been underestimated. However, there were not enough dense clusters or dense cell walls to introduce a large uncertainty; if the true number in each dense cluster had been twice the number

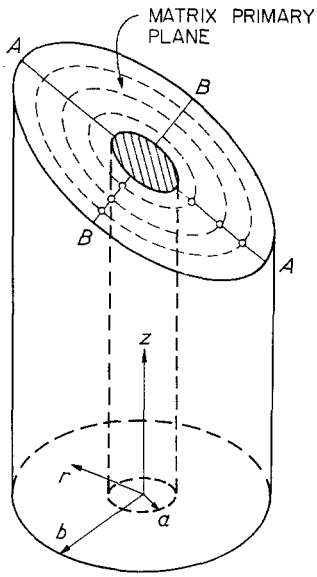

Figure 2 Geometry of the unit composite cylinder sectioned along the primary plane of the matrix.

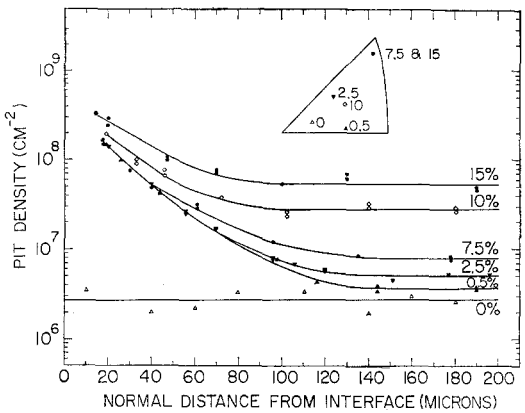

Figure 3 Pit density profiles on the matrix primary plane for as-grown specimens of various fibre fractions.

resolved, the average density would have been underestimated by only about 5% in the worst case. There was nothing to suggest that a large fraction of the individual pits actually represented unresolved multipoles. There were, however, unresolved pits in most of the sharp sub-boundaries. It was estimated that if these could have been counted in the composites they would have contributed a pit density in the neighbourhood of 10^7 cm^{-2}, which would have represented a substantial fraction of the total density in most cases. Although these dislocations could not be included in the count, it is felt the densities reported give a fair characterisation of the matrix in that the sharp sub-boundaries, being much more widely spaced than the cell walls, would not have a strong influence on matrix properties. Specimens etched after a small strain showed dislocation accumulation as thicker and more complete cell walls indicating that these were strong obstacles to dislocation motion.

Dislocation-density profiles for various fibre volume fractions are shown in fig. 3. Duplicate points at a given distance from the interface represent measurements along the major and minor axes in fig. 2 and were in good agreement indicating that the dislocation density was quite uniform around the fibre. In all the reinforced specimens, there was a pit density plateau in the body of the matrix up to roughly 100 μm from the interface and then the dislocation density increased as the fibre was approached. The pit density at any position tended to increase with fibre volume fraction overshadowing any differences due to the variation of the crystal orientation. The differences were greater in the plateau region, the curves tending to merge closer to the fibre. Even one fibre ($V_f = 0.5\%$) was apparently able to increase the dislocation density slightly and create incipient cell structure throughout the matrix, i.e. over distances of $\approx$ 1500 μm.

4. Discussion

The simple two-element model of fig. 2 is adequate for discussion of the present case of well-separated fibres since transverse stresses or strains are relatively low midway between the fibres and each fibre and its equivalent shell of matrix behaves almost independently. In this work, the fibre radius a was 114 μm and the radius b of the equivalent cylinder of matrix varied from 1590 μm at $V_f = 0.5\%$ to 290 μm at $V_f = 15\%$.

The enhanced dislocation densities arise in the plastic matrix strains attending thermal contraction and several simple models possibly pertinent here are shown schematically in fig. 4. The composite as solidified at T_0 (fig. 4a) would, if the tungsten wire and copper matrix were separated and free to contract individually, have at $T < T_0$ the dimensions in fig. 4b. The strains required at the interface total $\delta = (k_m - k_f)(T - T_0)$, where the k's are the thermal expansion coefficients ($\delta < 0$). It is assumed that transverse sections remain plane. Fig. 4c represents the difference taken up by elastic strains in the two elements while in fig. 4d it is supposed that the

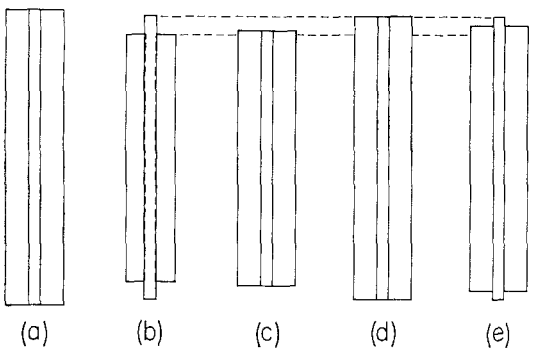

Figure 4 Accommodation of differential shrinkage in a two-element composite: (a) As solidified at T_0. (b) At $T < T_0$, if elements were free to contract independently. (c) Elements strained elastically. (d) Matrix flows plastically to relieve stresses. (e) Stresses relieved by plastic flow of matrix and by interface shear.

soft matrix has flowed plastically to conform to the length and diameter assumed by the wire in the unstrained state at T, internal stresses being completely relaxed. It seems also necessary to include the case, fig. 4e, where relaxation of the axial stresses has occurred partly by fibre-matrix interface shear as well as by general plastic flow of the matrix. The transverse stresses cannot be relaxed except by flow of the bulk of the matrix.

4.1. Matrix Plastic Strain

The copper matrix is very soft and the final δ is near 1 % so that the model of essentially complete relaxation by matrix flow, fig. 4d, might be thought to give a close approximation to the plastic strains. The axial plastic strain in the matrix e_z is $-\delta$, and the constancy of volume condition for the plastic state requires the matrix cross-section to be reduced by this amount. The inner radius of the matrix must expand by a length $-\delta a$, whence for case 4d the plastic strains in the matrix are calculated as:

$$e_z = -\delta \tag{1a}$$

$$e_r = -\delta(-3a^2/2r^2 - \tfrac{1}{2}) \tag{1b}$$

$$e_\theta = -\delta(3a^2/2r^2 - \tfrac{1}{2}) \tag{1c}$$

The outer radius of the matrix does not enter and these strains do not vary with fibre fraction. The transverse strains are large up to about one fibre diameter from the interface (after which they are near $\delta/2$ which merely represents the lateral contraction accompanying the constant axial extension) and so would explain dislocation densities near the fibre in excess of the constant increase produced by e_z. However, the prediction that strain at any r, hence dislocation density, will be independent of fibre fraction is contrary to the observed strong dependence on V_f of the dislocation density in the body of the matrix. It is suggested below that this discrepancy arises because there is shear in the matrix adjacent to the interface, as in fig. 4e, and the axial strain is not correctly given by equation 1a but is lower and varies with fibre fraction. The dislocation densities in fig. 3 are seen as a combination (not necessarily a linear one) of the fibre-fraction-independent contribution near the fibre from transverse strains, as described above, and a fibre-fraction-dependent contribution throughout the matrix from the axial strain. Before examining the axial strain, the elastic stresses induced by cooling before the beginning of matrix flow are considered.

4.2. Elastic Solution

The stresses in the two-element composite cylinder of isotropic components have been calculated by Poritsky [9]. It is sufficient for the present purpose to use the solution for the case where the Poisson's ratios of the two components are equal. The principal stresses in the matrix as obtained from Poritsky's solution (there are misprints in the original article in the expressions for the coefficients) have been given elsewhere [10] as:

$$\sigma_r^m = -[E_m\delta/(1 + \alpha + \alpha\beta H)][(a/b)^2 - (a/r)^2] \tag{2a}$$

$$\sigma_\theta^m = -[E_m\delta/(1 + \alpha + \alpha\beta H)][(a/b)^2 + (a/r)^2] \tag{2b}$$

$$\sigma_z^m = -[E_m\delta/(1 + \alpha + \alpha\beta H)][2\nu(a/b)^2 + (1 + \alpha + \alpha\beta H)/(1 + \beta H)] \tag{2c}$$

where E_f and E_m are the Young's moduli of fibre and matrix, ν is the Poisson's ratio of both, $H = E_m/E_f$, $\alpha = a^2(1 - 2\nu)/b^2$, $\beta = (b^2/a^2 - 1)$ and the other quantities are as previously defined. Numerical values appropriate to the present situation were $E_f = 39.2 \times 10^3$ kg/mm^2 (as measured), $E_m = 10.5 \times 10^3$ kg/mm^2 (calculated for the orientation of the 10% V_f specimen), 4.9×10^{-6} and 19.7×10^{-6} per °C for k_f and k_m respectively near 500°C, and $\nu = 0.3$.

The stresses calculated for a temperature change of 1°C at $V_f = 0.5$ and 10%, representative of a low and a higher V_f in the present work, are shown in fig. 5 as functions of distance from the fibre-matrix interface (i.e. from $r/a = 1$). The transverse stresses σ_r and σ_θ are relatively insensitive to b, i.e. to V_f. It is seen from the

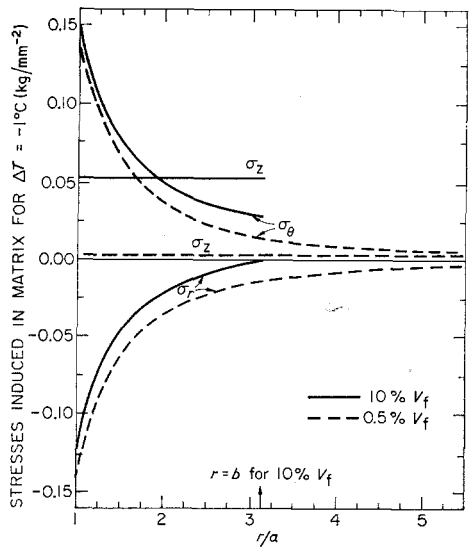

Figure 5 Matrix principal stresses in the elastic state calculated from equation 2 for a temperature decrease of 1°C.

magnitudes of the principal stresses in fig. 5 that only a 1°C temperature change would have been able to induce shear stresses of $\sim$ 100 gm/mm^{-2}, more than sufficient to produce plastic flow of the matrix the micro-yield stress of which was 50 gm/mm^{-2} at room temperature.

4.3. Role of Interface Shear

For the axial stresses, the limit to which these build up may be determined not by general flow of the matrix but by longitudinal plastic shear along the fibre-matrix interface. The axial tension in the matrix is determined by the compression in the fibre, $\sigma_z^f = \sigma_z^m (1 - b^2/a^2)$ (3). The load which develops σ_z^f is transmitted by shear stresses on the interface, and these cannot rise above the matrix shear yield stress, τ_0. This yield stress sets an upper limit for the axial stress in the fibre (and thus in the matrix), any continued tendency for the axial stress to rise above this during cooling being relieved by continued interface shear. In this limit the load in the fibre is built up linearly over a length $l_c = a\sigma_z^f{}_{max}/\tau_0$ [11]. If τ_0 were as much as 10 gm/mm^{-2} at elevated temperatures, the load transfer length in centimetres would be about equal to $\sigma_z^f{}_{max}$ in kg/mm^2. The few centimetres available for load transfer in the specimen limit the effective σ_z^f to $\lesssim$ 1 kg/mm^{-2}. The axial stress in the matrix is thus limited to lower values at lower V_f, where b in equation 3 is larger. The value of δ at which the limit of σ_z^f is reached happens to correspond to about a 1°C cooling interval for all fibre fractions. Thus the axial matrix stresses plotted in fig. 5 represent their limiting values from load-transfer considerations.

From these considerations, qualitative predictions concerning the amount of plastic strain produced by the axial matrix stress (thus concerning the plateau dislocation density) are made as follows. At $V_f = 0.5\%$, the matrix axial stress limit from fig. 5 is only a few gm/mm^{-2}, enough to cause only slow creep in the body of the matrix hence only a slight rise in plateau dislocation density. At $V_f = 10\%$, however, the calculated matrix axial stress limit is well above the high temperature yield stress and thus allows build-up of σ_z^m to levels sufficient for steady plastic flow and substantial plastic strain. Thus at higher V_f, a higher fraction of the axial differential shrinkage δ will be accommodated by general matrix flow and a smaller fraction by interface shear, and the plateau dislocation density will tend to rise with increasing V_f.

It is thought that the interface shear was localised within the matrix zone close to the fibre where etch pit observations could not be made and that the high dislocation densities observed at small distances from the fibre were the result of the transverse plastic flow of the matrix. The substitution of interface shear for axial plastic strain modifies equation (1); at the point where axial plastic strain is zero, the transverse plastic strains become: $e_r = \delta a^2/r^2$, $e_\theta = -\delta a^2/r^2$ (4), the constancy-of-volume term $\delta/2$ in equations 1 having shrunk to zero and the coefficient of the $1/r^2$ term having decreased by $\frac{1}{3}$. At small distances from the fibre where they are important, it thus appears that the transverse strains change relatively little with a variation in interface shear accompanying a variation of fibre fraction so that the contribution of these strains to enhancement of dislocation density would be only weakly dependent on fibre fraction. It is thus supposed that (a) the rapid fall of dislocation density with distance to the plateau in fig. 3 corresponds to the $1/r^2$ decay of the transverse plastic strains (equations 1 and 4) to a level where they make no contribution detectable above the plateau value determined by the axial strain, and (b) the upward shift with increasing V_f of the dislocation density curves near the fibre mainly reflects the presence of the plateau contribution.

4.4. Cell Structure

Although the enhanced dislocation density produced at high temperatures would have been reduced by the annealing taking place during cooling, this is not likely in the present case to have reduced the dislocation density to a low level except in the initial stage of cooling in view of the findings of many investigators that effective reduction of the dislocation density of as-grown copper crystals requires annealing at 1000° C or higher. It seems likely that dislocations produced at high temperatures are partly annealed out but partly combined in metastable arrangements and the accumulation of these arrangements through most of the 1050° C cooling range builds up the cell structure observed at room temperature, somewhat as though the specimen had been subjected to a high temperature creep test. The formation of cell structure would be favoured by the multiple-glide conditions prevailing in the matrix judging from the evidence that rough cell structures can be formed after small axial strains ($\sim 10^{-3}$) at room temperature in copper crystals of multiple-glide orientations [8, 12]. The narrow sub-boundaries with much larger spacing are thought to have been present immediately after solidification and to have arisen during the freezing process in the same way as in unreinforced crystals.

4.5. Other Studies

The present work shows that a metal-matrix composite may have as fabricated a prestrained matrix with an enhanced dislocation density which increases with fibre fraction and thus is likely to have deformation properties quite different from the unreinforced matrix. The large difference in thermal expansion coefficients, the large cooling range involved and the very soft single crystal matrix tended to exaggerate the effect here. However, some effect would normally be expected. That Pinnel and Lawley [3] saw no enhanced dislocation density in aluminium-stainless steel fibre composites away from the fibre may be attributed in part to their special processing procedure (cooling under pressure to a low temperature) and their use of high-purity aluminium which has a low recovery temperature.

The copper single crystal-tungsten system was studied by Kelly and Lilholt [13] who did not make structure observations but found high derived matrix strain-hardening rates in Stage II of composite deformation which they attributed to plastic constraint of the matrix so that part of the matrix strained elastically. Since they used 10 and 20 μm wires and included higher fibre fractions, the present observations of initial structure would not be directly applicable to their results. However, the implication is that their specimens also would have had high initial dislocation densities and possibly cell structures which may have had much to do with the high matrix strain hardening rates. Current observations on specimens strained 10^{-4} or greater in the present work do not support the contention that part of the matrix remains elastic, i.e. as close to the fibre as observations can be made, the dislocation density increases. However, it is likely that the initial microyielding begins over the plateau region of fig. 3 while the zone of high-density near the fibres has a higher microyield stress and is still elastic.

Acknowledgements

This work was supported in part by the US Atomic Energy Commission contract AT(11-1)-1198 through the Materials Research Laboratory. The authors are indebted to J. B. Woodhouse for advice on scanning microscopy and to A. P. Boresi for reading the manuscript.

References

1. J. R. HANCOCK, *J. Composite Materials* **1** (1967) 136.
2. J. R. HANCOCK and J. C. GROSSKREUTZ, *Metal Matrix Composites, ASTM STP* **438** (1968) 134.
3. M. R. PINNEL and A. LAWLEY, *Met. Trans. AIME* **1** (1970) 1337.
4. G. GARMONG and L. A. SHEPARD, *ibid* **2** (1971) 175.
5. F. W. YOUNG and J. R. SAVAGE, *J. Appl. Phys.* **35** (1964) 1971.
6. J. W. MITCHELL, J. C. CHEVRIER, B. J. HOCKEY, and J. P. MONAGHAN, JR. *Canad. J. Phys.* **45** (1967) 453.
7. A. K. N. REDDY and H. WILMAN, *Trans. Inst. Metal Finishing* **36** (1959) 97.
8. J. D. LIVINGSTON, *Acta Metallurgica* **10** (1962) 229.
9. H. PORITSKY, *Physics* **5** (1934) 406.
10. A. W. HULL and E. E. BURGER, *ibid* **5** (1934) 384.
11. A. KELLY and G. J. DAVIES, *Metallurgical Reviews* **10** (1965) 1.
12. J. LANKFORD, JR. Ph.D. Thesis, University of Illinois, 1969.
13. A. KELLY and H. LILHOLT, *Phil. Mag.* **20** (1969) 311.

Received 5 July and accepted 4 August 1971.